Theoretical predictions of structures in dispersions containing charged colloidal particles and non-adsorbing polymers

Xie, Fei; Turesson, Martin; Woodward, Clifford E.; Van Gruijthuijsen, Kitty; Stradner, Anna; Forsman, Jan

Published in:
Physical Chemistry Chemical Physics

DOI:
10.1039/c5cp07814h

2016

Journal Name

ARTICLE TYPE

Cite this: DOI: 10.1039/xxxxxxxxxx

Theoretical predictions of structures in dispersions containing charged colloidal particles and non-adsorbing polymers†

Fei Xie,*[a], Martin Turesson[a], Clifford E. Woodward[b], Kitty van Gruijthuijsen[c], Anna Stradner[d] and Jan Forsman [a]

Received Date
Accepted Date

DOI: 10.1039/xxxxxxxxxx

www.rsc.org/journalname

We develop a theoretical model to describe structural effects on a specific system of charged colloidal polystyrene particles, upon the addition of non-adsorbing PEG polymers. This system has previously been investigated experimentally, by scattering methods, so we are able to quantitatively compare predicted structure factors with corresponding experimental data. Our aim is to construct a model that is coarse-grained enough to be computationally manageable, yet detailed enough to capture the important physics. To this end, we utilize *classical* polymer density functional theory, wherein all possible polymer configurations are accounted for, subject to a mean-field Boltzmann weight. We make efforts to counteract drawbacks with this mean-field approach, resulting in structural predictions that agree very well with computationally more demanding simulations. Electrostatic interactions are handled at the fully non-linear Poisson-Boltzmann level, and we demonstrate that a linearization leads to less accurate predictions. The particle charge is an experimentally unknown parameter. We define the surface charge such that the experimental and theoretical gel point at equal polymer concentration coincide. Assuming a fixed surface charge for a certain salt concentration, we find very good agreement between measured and predicted structure factors across a wide range of polymer concentrations. We also present predictions for other structural quantities, such as radial distribution functions, and cluster size distributions. Finally, we demonstrate that our model predicts the occurrence of equilibrium clusters at high polymer concentrations, but low particle volume fractions and salt levels.

1 Introduction

Aqueous colloidal dispersions are widely applied in food products and other materials, for example paint, ink and coatings[1]. Colloidal particles usually interact with each other via short-ranged van der Waals (vdW) attractions, and when this attraction is strong, the system may form a gel[2,3]. Colloidal gels find a variety of applications as well[4]. , where the attractions can originate from rather different sources, such as vdW interactions, hydrophobic/patchy interactions, the addition of non-adsorbing polymer, or the addition of adsorbing/bridging polymers. A colloidal dispersion with non-adsorbing polymers form an especially useful model system. Various theoretical models of particle-polymer mixtures have been utilized in previous work, aiming to quantify the various interactions and to establish how they affect the macroscopic properties[5–11]. Several experimental methods are available to elucidate the structure of particle-polymer mixtures, which can then be compared with the model predictions[12–20]. Most of them are based on some form of scattering, with light or neutrons. In this work, we develop a rather detailed theoretical model to study mixtures of colloidal particles and polymers. The system contains charged polystyrene particles that are grafted by a layer of poly(ethylene glycol) (PEG)-based surfactant, with a thickness wide enough to counteract particle-particle vdW attractions[21]. Thus, the steric repulsion between the polymer shells effectively stabilizes the particles against vdW attractions[22,23]. Non-adsorbing PEG polymers are added to induce attractions between the particles, in a controlled way. In the vicinity of particle surfaces, the polymer excess chemical potential will increase, as a result of configurational restrictions. This means that, at equilibrium, the ideal chemical potential, i.e. the polymer concentration, will drop. Hence, interparticle regions will

[a] *Theoretical Chemistry, Lund University, P.O.Box 124, S-221 00 Lund, Sweden. Fax: +46468225; Tel.:+46462220381; E-mail: fei.xie@teokem.lu.se*
[b] *School of Physical, Environmental and Mathematical Sciences, University College, University of New South Wales, ADFA, Canberra ACT 2600, Australia.*
[c] *Adolphe Merkle Institute, University of Fribourg, Chemin des verdiers 4, CH-1700 Fribourg, Switzerland. Current address: Firmenich SA, Meyrin, Switzerland*
[d] *Physical Chemistry, Lund University, P.O.Box 124, S-221 00 Lund, Sweden.*
† Electronic Supplementary Information (ESI) available: [In the ESI, we list experimental data that are required to establish the resolution function, $R(q,Q)$. We also present some electrostatic interaction free energies, between charged flat surfaces.]

be depleted of polymers, and are pushed together by the resulting differences in osmotic pressure. The strength of this attraction increases with polymer concentration. In a good solvent, the range of the depletion interaction is related to polymer size at low concentrations, and to the correlation length in the semi-dilute regime (i.e, at higher polymer concentrations). Our theoretical model to describe this system is relatively detailed, in the sense that the polymers are explicitly modelled, and all possible configurations of the model polymers are accounted for, subject to a mean-field Boltzmann weight. We shall then utilize *classical* polymer density functional theory (DFT). Nevertheless, the solvent will be treated implicitly. Electrostatic interactions are handled at the full non-linear Poisson-Boltzmann (PB) level. The combination of DFT and PB allows us to establish the interaction free energy between large and flat surfaces. Using the Derjaguin approximation[24], which is expected to be highly accurate for the investigated systems, we obtain a spherically symmetric potential of mean force (PMF) acting between the particles. This PMF is then imported into a simple Metropolis Monte Carlo program, and a subsequent simulation allows us to obtain theoretical predictions of structural properties. These predictions are then directly compared with corresponding results, from scattering experiments.

The computational advantages of importing polymer and ion mediated potential of mean forces (PMF:s), rather than treating these explicitly, are quite dramatic. Still, the approach naturally has some limitations. First, we note that the strategy would fail for systems in which the polymers are larger than, or similar to, the particles (as measured by the correlation length). The Derjaguin Approximation will then no longer be accurate for the pair PMF, and there will in general be a significant influence from many-body interactions. Another obvious limitation with our approach is that the use of standard MC simulations will prevent any dynamical predictions. One could in principle consider dynamical methods, but these would most likely turn out to be very expensive computationally. Furthermore, as we will show, some systems display quite large free energy barriers, implying slow dynamics. Thus, at least at this stage, we have limited our scope to structural investigations.

2 Model and theory

The experimental particle-polymer mixture consisted of polystyrene particles that were surface-grafted by Tween 80 (a PEG-based surfactant) and acrylic acid groups, together with dissolved PEG polymers. The particles were synthesized using emulsion polymerization and purified by solvent exchange, which was also used to create a well-defined salt concentration in the concentrated stock dispersions. The synthesis and characterization of the particles, denoted MA3, has been described before, giving a radius of about 0.06 μm, with a polydispersity below 15 %, and a steric layer thickness of about 40 Å. The latter serves to counteract attractive dispersion (vdW) interactions. The PEG polymers, with a reported molecular weight of 13.3 kg/mol and a polydispersity index of 1.08, were purchased from Polymer Source. We used a previously established empirical relation to estimate the polymer radius of gyration: $R_g = 47$ Å, from the molecular weight[25]. The particles and polymers were prepared by vortex mixing, with salt concentrations in the continuous phase adjusted to 50 mM or 1.5 mM of monovalent salt ($NaCl$ and/or NaN_3). Hence, the electrostatic particle interactions have a short (50 mM) or intermediate (1.5 mM) range. The structure of the particle-polymer mixtures was characterized by small angle neutron and X-ray scattering (SANS and SAXS), at the Paul Scherrer Institute, Switzerland. Details of these measurements have been provided elsewhere[21,26]. The measured 2D scattering patterns were corrected for background scattering, and radially averaged to obtain angle-dependent scattering intensity curves, $I(q)$. In order to obtain the structure factors, $S(q)$, of concentrated particle dispersions, the intensity curves measured by SANS or SAXS were divided by the intensity curve for a non-structured dilute sample, with corrections for the concentration difference. SAXS has the advantage over SANS that the angular resolution is much higher, yielding essentially unsmeared $S(q)$ curves. The addition of PEG significantly changes the scattering length of the continuous solvent phase. Though this can be easily corrected for in SANS, we could not obtain reliable structure factors from the SAXS data at high polymer concentrations. Therefore, SAXS data are used to model pure particle dispersions, while SANS data are used for the particle-polymer mixtures.

In order to address this system theoretically, we shall use the same polymer model as was adopted in our previous work[27], where we developed a simulation model for PEG in aqueous solutions, at room temperature. Specifically, it is based on a pearl-necklace polymer representation, where each monomer ($-CH_2-CH_2-O-$) is represented by a single hard-sphere bead, of diameter d. These beads are connected by bonds that are orientationally flexible, but have a fixed length b. Thus our model only contains two adjustable parameters, d and b, which are the same for all polymer lengths and concentrations. These parameters were adjusted so that experimental values for radii of gyrations and osmotic pressures are reproduced, for a large range of polymer lengths and concentrations. Further details can be found in ref.[27]. Here, we merely state that the final fitted values, for the simulation model, was $d = 2.65$ Å and $b = 4$ Å.

Depletion attractions between the particles can be induced by adding polymers, and the modest polymer size ensures that the depletion-induced attractions are short-ranged compared to the particle radius. The depth of the attractive potential is controlled by the polymer concentration, and since the attraction is short-ranged, colloidal gels are formed at some threshold polymer concentrations[3,28–30].

In this work, predictions of polymer-induced interactions will be established by *classical* polymer DFT. Here, the free energy is minimized, as a function of the polymer density distribution. In this way, the equilibrium monomer density profile is established, subject to a mean-field approximation, where the mean field is provided by the monomer density distribution itself. Details of polymer DFT, and how to implement it in an efficient manner, can be found elsewhere[31–33]. Here we only include a brief summary.

The exact canonical free energy density functional, $\mathscr{F}^{id}$, for an

ideal and flexible r-mer polymer fluid is given by

$$\beta\mathscr{F}^{id} = \int N(\mathbf{R})\left(\ln[N(\mathbf{R})]-1\right)d\mathbf{R} + \beta\int N(\mathbf{R})\Phi^{(b)}(\mathbf{R})d\mathbf{R} + \beta\int n(\mathbf{r})V_{ext}(\mathbf{r})d\mathbf{r} \quad (1)$$

where $\beta = 1/(kT)$ is the inverse thermal energy and $n(\mathbf{r})$ is the monomer density, at coordinate $\mathbf{r}$. We denote a polymer configuration as $\mathbf{R} = (\mathbf{r}_1, ..., \mathbf{r}_r)$, i.e. $N(\mathbf{R})$, is proportional to the probability of configuration $\mathbf{R}$. The bonding potential, $\Phi^{(b)}(\mathbf{R})$, describes connectivity along the chain:

$$\Phi^{(b)}(\mathbf{R}) = \sum_{i=1}^{r-1}\phi^{(b)}(|\mathbf{r}_i - \mathbf{r}_{i+1}|) \quad (2)$$

$V_{ext}(\mathbf{r})$ is an external potential acting (equally) on all monomers (in our case stemming from the particle surfaces). For interacting monomers, there will also be an excess term, $\mathscr{F}^{ex}$. We will assume that this is a functional of the monomer density, $n(\mathbf{r})$. Specifically, we will utilize the Generalized Flory Dimer (GFD) expressions[32,34] for the entropic penalty associated with hard core excluded volume. Following Nordholm and co-workers[35], we account for non-local excluded volume effects via a coarse-grained (weighted) monomer density:

$$\bar{n}(\mathbf{r}) = \frac{3}{4\pi d_{DFT}^3}\int_{|\mathbf{r}-\mathbf{r}'|<d_{DFT}} n(\mathbf{r}')d\mathbf{r}' \quad (3)$$

where d_{DFT} is the monomer hard sphere diameter. The polymer chemical potential, μ_p, is composed of an ideal (μ^{id}) and an excess (μ^{ex}) term:

$$\mu_p = \mu^{id} + \mu^{ex} \quad (4)$$

The total grand potential functional, Ω, is given by

$$\Omega = \mathscr{F}^{id}[N(\mathbf{R})] + \mathscr{F}^{ex}[n(\mathbf{r})] - \mu_p\int N(\mathbf{R})d\mathbf{R} \quad (5)$$

This implies the following equilibrium distribution:

$$N_r(\mathbf{R}) = e^{\beta\mu^{id}}\prod_{i=1}^{r-1}T(|\mathbf{r}_i - \mathbf{r}_{i+1}|)\prod_{i=1}^{r}e^{-\psi(\mathbf{r}_i)} \quad (6)$$

where:

$$\psi(\mathbf{r}) \equiv \frac{\delta\beta\mathscr{F}^{ex}}{\delta n(\mathbf{r})} + \beta V_{ext}(\mathbf{r}) - \beta\mu^{ex} \quad (7)$$

With freely rotating bonds of fixed length, b_{DFT}, the bonding kernel reads:

$$T(|\mathbf{r}-\mathbf{r}'|) = \delta(|\mathbf{r}-\mathbf{r}'| - b_{DFT}) \quad (8)$$

The total monomer density is obtained from:

$$n(\mathbf{r}) = \int\sum_{i=1}^{r}\delta(|\mathbf{r}-\mathbf{r}_i|)N(\mathbf{R})d\mathbf{R} \quad (9)$$

It is convenient to introduce chain propagator functions, $c(i;\mathbf{r})$. These are related by a recursion formula:

$$c(i;\mathbf{r}) = e^{-\psi(\mathbf{r})}\int c(i-1,\mathbf{r}')T(|\mathbf{r}'-\mathbf{r}|)d\mathbf{r}' \quad (10)$$

with boundary condition $c(0;\mathbf{r}) = 1$. This allows us to formulate the density as:

$$n(\mathbf{r}) = e^{\beta\mu^{id}}\sum_{i=1}^{r}\int c(r-i;\mathbf{r})T(|\mathbf{r}-\mathbf{r}'|)c(i;\mathbf{r}')d\mathbf{r}' \quad (11)$$

In many cases, the theory has proven remarkably accurate, yet exceptionally fast in comparison with Monte Carlo and Molecular dynamics simulations, especially in flat (or spherical) geometries.[36] The computational benefits, combined with the grand canonical formulation, means that (for instance) polymer induced surface interactions can be studied in systems with realistic degrees of polymerizations. In fact, previous studies include surface interactions in the presence of semi-flexible 20 000-mers.[33] Such systems are of course impossible to handle by simulation methods. Nevertheless, polymer DFT is still based on a mean-field assumption, and it is well-known that such theories are unable to properly account for intramolecular interactions. One consequence of this is an erroneous prediction of how the radius of gyration scales with polymer length, in a good solvent. On the other hand, at high polymer concentrations, the mean-field assumption is quite reasonable. We suggest the following approach, to counteract the mean-field problems at low concentrations, yet retain its advantages and accuracy at high concentrations. As already mentioned, we denote the hard-sphere diameter and bond length used in the DFT treatment as d_{DFT} and b_{DFT}, respectively. We choose b_{DFT} such that the low concentration mean-field prediction agrees with the experimental R_g value (47 Å), for the given degree of polymerization, r. With a monomer molecular weight of 44 g/mol, and a polymer weight of 13300 g/mol, we arrive at $r \approx 13300/44 \approx 300$. Hence, the mean-field prediction of single polymer radius of gyration, $R_g(DFT)$, is $R_g(DFT) = b_{DFT}\sqrt{300/6}$. Equating this to the experimental value of 47 Å, we arrive at $b_{DFT} \approx 6.65$ Å. This will ensure that the DFT predicts the correct single polymer radius of gyration. Keeping this parameter fixed, we adjust d_{DFT}, for each polymer concentration, so that the corresponding experimental bulk osmotic pressure, Π_{exp}, is reproduced. The latter is estimated by a semi-empirical equation of state (EOS), suggested by Cohen et al.[37] The DFT predictions for osmotic pressure, $\Pi_{DFT}(d_{DFT})$ is obtained via a Generalized Flory-dimer treatment of the excluded volume[32,38]. Our chosen value for d_{DFT} is thus obtained from the relation $\Pi_{DFT}(d_{DFT}) = \Pi_{exp}$ (at each investigated polymer concentration). Since the DFT fulfills the so-called contact value theorem, this approach will ensure that the polymer pressure exerted against a surface, is given by the "correct" osmotic pressure, i.e. close to experimental values. We have evaluated our suggested approach, by comparing DFT predictions of monomer density profiles outside a non-adsorbing inert hard surface, with corresponding results from simulations of our previously established PEG model[27] ($b = 4$ Å, $d = 2.65$ Å). We find an excellent agreement, both at low and high polymer concentrations, as shown in Figure 1. Given that the "reference" simulation model has been shown to reproduce experimental values for osmotic pressure and radius of gyration with a very high accuracy, across many orders of magnitude in terms of concentration and polymer length, we expect

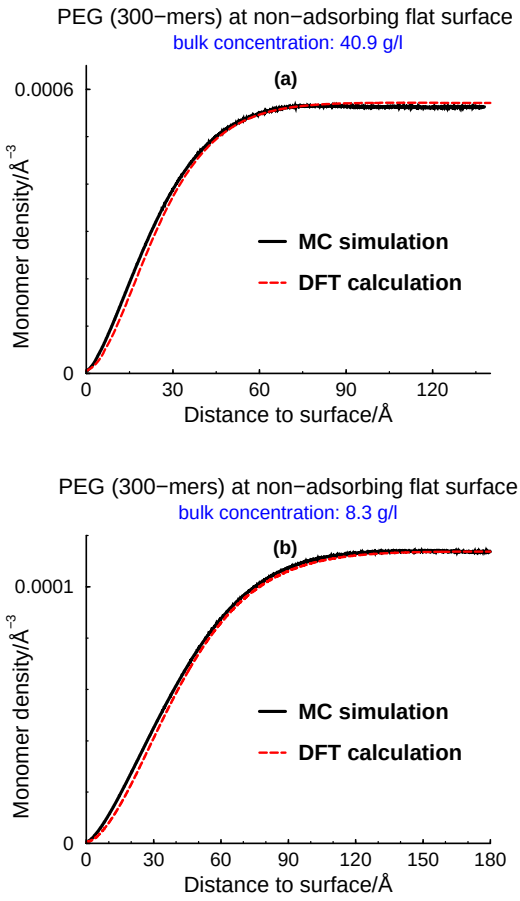

Fig. 1 Monomer density profiles outside an inert hard surface, for our 300-mer PEG models. The dashed lines are from DFT calculations, whereas the solid black lines are results from MC simulations, using our previously established model for PEG[27], in aqueous solution at room temperature. Two different bulk polymer concentrations (c_p^b) have been investigated, corresponding to typical "low" and "high" values in this work.
(a) A high bulk polymer concentration, $c_p^b = 40.9$ g/L
(b) A low bulk polymer concentration, $c_p^b = 8.3$ g/L

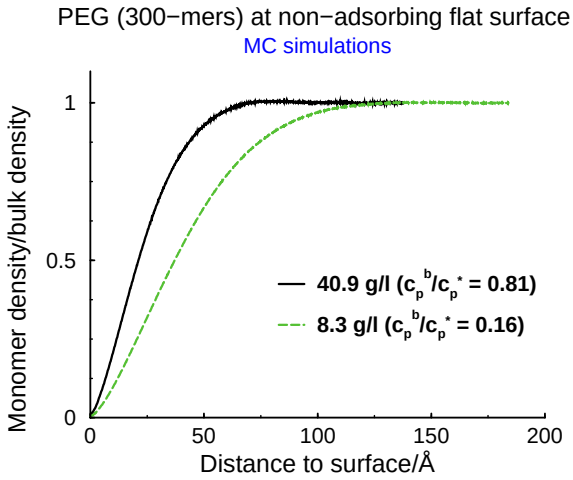

Fig. 2 The same simulated monomer density profiles as in Figure 1, but normalized by their respective bulk density, thus highlighting how the depletion layer drops with density.

that our DFT calculations will provide highly accurate measures of polymer-induced depletion interactions.

It is of some interest to compare the investigated polymer concentrations with the overlap concentration, c_p^*. One problem is that the latter lacks an unambiguous definition. We will consider two options, with ρ_p denoting the number density of polymers:

1. With a simple cubic lattice model, where each polymer occupies a lattice site, one readily arrives at $\rho_p^*(2R_g)^3 = 1$. This leads to $c_p^* \approx 26$ g/L.

2. If we consider each polymer as occupying a spherical volume, we can instead find an estimate of the overlap concentration by equating the radius of gyration to the radius of the sphere: $\rho_p^* 4\pi R_g^3/3 = 1$. This gives us $c_p^* \approx 50$ g/L.

These definitions have also been discussed by Ying and Chu[39]. Thus, the case of "low" concentration, in Figure 1 (b) is considerably below c_p^*, irrespective of definition, whereas the "high" concentration (Figure 1 (a)) is perhaps best described as "close to" the overlap concentration. Scanning the polymer literature, the second definition seems to be most commonly used, so we shall henceforth stipulate that $c_p^* \approx 50$ g/L, although there are reasons to keep in mind that this is a very approximate measure.

In Figure 2, we demonstrate how the thickness of the depletion layer, i.e. the range of the depletion attraction, drops as the concentration increases. In approximate polymer theories, it is not uncommon to assume that the polymer correlation length essentially equals the radius of gyration, all the way up to, and beyond the overlap concentration, c_p^*. However, it is clear from Figure 2 that the correlation length starts to drop at concentrations considerably below that value.

As mentioned earlier, the investigated colloidal particles MA3 had a hard-sphere radius, R_c, of about 600 Å. Since this is more than an order of magnitude larger than R_g, we can safely rely upon the Derjaguin approximation[24] (DA) for these systems, i.e.

in practice we use DFT to establish the corresponding interaction free energies per unit area, $g(D)$, between infinite parallel and flat surfaces, separated by D. According to the DA, the force $F(D)$ acting between particles at surface separation D, can be written as:

$$F(D) = \pi R_c g(D) \tag{12}$$

The corresponding potential of mean force (PMF), denoted W, is then obtained by integration:

$$W(D) = -\pi R_c \int_D^\infty g(x)dx \tag{13}$$

As already mentioned, there are two different contributions to the overall PMF (in addition to the hard core interaction). The non-adsorbing polymers mediate attractive depletion interactions, which are counteracted by electrostatic double-layer forces. The latter are obtained at the full non-linear Poisson-Boltzmann level, although we prefer a DFT formulation (integral equations)[40], rather than the corresponding (equivalent) non-linear differential equation.

One problem that arises with our approach, is that with the grand canonical formulation that is inherent to the DFT, we need an estimate of the polymer concentration in the "free volume" of the dispersion, i.e. the effective bulk polymer concentration. We have estimated this concentration in a self-consistent manner. For each choice of overall average polymer number concentration ρ_p in the dispersion [*], i.e. the number of polymers per unit volume of colloidal dispersion, we can estimate the bulk polymer concentration, ρ_p^b (in the "free volume") as:

$$\rho_p^b = \frac{\rho_p}{1 - N_c \frac{4\pi(R_c+\delta)^3}{3}} \tag{14}$$

where N_c denotes the number of collodal particles, and δ is a "depletion thickness". The latter can be calculated from the predicted (via DFT calculations) equilibrium monomer density distribution, $n_m(z)$, for our flat surface model:

$$\delta = \int_0^\infty (1 - n_m(z)/n_m^b)dz \tag{15}$$

where the z direction is perpendicular to the isolated flat surface, and n_m^b is the assumed bulk monomer density. These calculations are repeated until self-consistency is obtained, i.e. until $\rho_p^b = n_m^b/r$, where $r = 300$ is the degree of polymerization.

2.1 Comparing with AO theory

A simpler alternative to our suggested polymer DFT + fully non-linear PB approach, is to estimate the polymer depletion via the Asakura-Oosawa (AO) model[41,42], combined with a linearized PB level (screened Coulomb interactions) for electrostatics. A significant advantage is that the expressions for the PMF:s are analytic.

The AO theory offers a simplified treatment of polymers in theta solvents, where the chains generally are modelled as ideal, i.e. composed of point-like monomers, which are expelled from particles, but mutually non-interacting. In the AO approach, coarse-graining is taken one step further, and these ideal polymers are treated as penetrable spheres, with a radius that matches the polymer radius of gyration. While simple, the basic physics of depletion is captured by this model, and studies based on these concepts have led to a significantly deeper understanding of this mechanism[43–48]. Furthermore, mean-field approaches based on penetrable spheres have provided simple ways to predict general phase behaviours in systems where attractions are generated by depletion[49,50]. Nevertheless, for our system the AO polymer model has several drawbacks. Treating polymers as spherical objects is by itself a crude approximation, as is a neglect of polymer shape fluctuations[9–11,51]. We also note that water is a good solvent for PEG, i.e., even the ideal polymer model that the AO aims to simplify, is inappropriate for our system. For instance, the AO approach fails to capture the drop in correlation length that results when the polymer concentration is increased. An added advantage of the polymer model that we will utilize is that it has been shown to reproduce experimental osmotic pressure data of PEG+water solutions quite accurately, across many orders of magnitude in terms of polymer concentration[52].

This is highlighted in Figure 3, where we compare AO and DFT predictions of depletion interactions, at two different polymer concentrations. As we shall see, these concentrations are strong enough (experimentally) to generate gelation at high (50 mM) and low (1.5 mM) salt concentrations, respectively. We see that the AO and DFT generate similar predictions at the low polymer concentration, although the latter has a slightly longer range. At the high concentration, the DFT predicts a significantly diminished range of the depletion interaction, as a result of a reduced correlation length. On the other hand, excluded volume effects lead to a higher osmotic pressure than generated by ideal chains at the same concentration. Neither of these effects are captured by the AO theory, which explains why the corresponding PMF:s cross, i.e.the DFT predicts a stronger, but more short-ranged depletion interaction than the AO theory. In passing, we mention that the DA is expected to be accurate for the depletion interactions, as demonstrated in an earlier study[51].

2.2 Comparing with a linearized Poisson-Boltzmann treatment

Now we switch focus to the electrostatic PMF:s. In what follows, we shall treat the particles as being positively charged, even though experiments clearly have shown that they are negative. The reason is that positive charges simplify the discussion, avoiding tedious formulations, such as an "increased absolute valency". Given that the particles are weakly charged, we anticipate that the linearized PB generates an electrostatic potential decay that well matches predictions by the full PB. This is indeed the case, as we shall demonstrate below. However, this does not mean that the corresponding electrostatic PMF:s also agree. Specifically, as two charged surfaces, or large particles approach, the intersurface region will eventually be almost completely dominated by counterions. This alters the overall screening, and a linearized

[*] Overall polymer number and mass concentrations are denoted by ρ_p and c_p, respectively. The corresponding notation from bulk ("free volume") concentrations are ρ_p^b and c_p^b, respectively

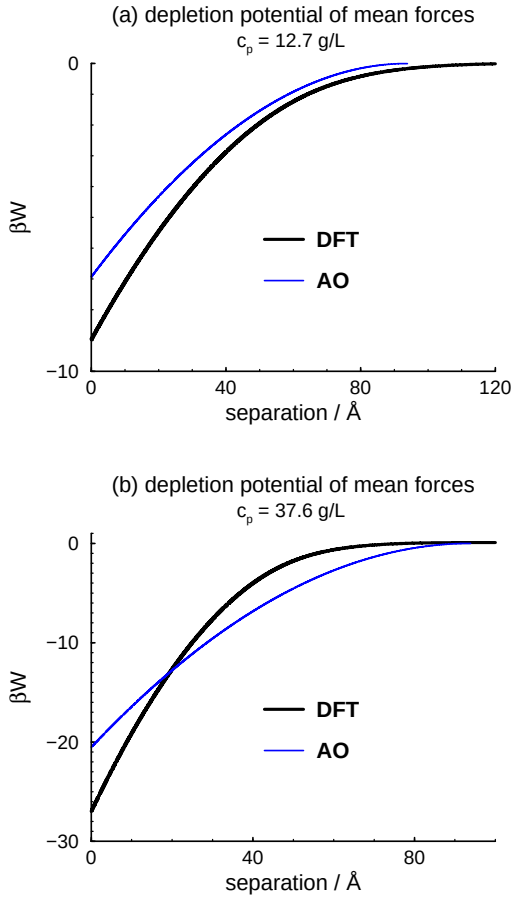

Fig. 3 Polymer-induced potential of mean forces between two particles, as predicted by DFT and AO theory, at two different polymer concentrations. When calculating the bulk polymer concentration, we have assumed a particle volume fraction $\phi_c = 0.215$
(a) $c_p = 12.7$ g/L
(b) $c_p = 37.6$ g/L.

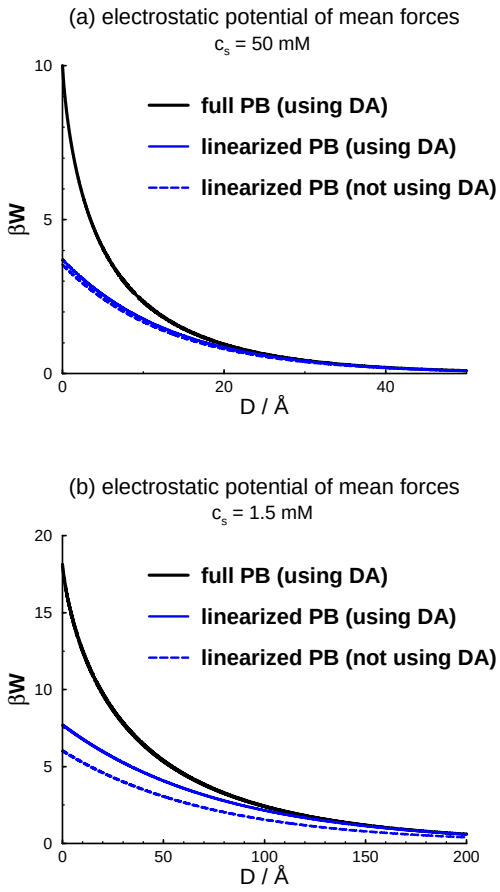

Fig. 4 Electrostatic PMF:s. Linearizing the PB leads to screened Coulomb interactions. Dashed blue lines are W_{SC} as obtained directly from eq. (16), whereas solid blue lines are generated by applying the DA to planar surface SC predictions.
(a) $c_s = 50$ mM. The valency, $Z_c = 1100$, matches the value used in our studies of gelation (see below), at this salt concentration.
(b) $c_s = 1.5$ mM. The valency, $Z_c = 275$, matches the value used in our studies of gelation (see below), at this salt concentration.

screened Coulomb (SC) approach will be less accurate. The separation regime across which these effects are significant increases with the screening length, so we anticipate stronger deviations at low ionic strengths. This is corroborated in Figure 4, where we compare predictions from SC and PB approaches. The full PB option generates PMF:s that are considerably steeper than SC predictions at close separations, despite the agreement observed for single surface potential profiles (see below). The particle valencies used in Figure 4 match our optimized values (see below) at the two salt concentrations, namely $Z_c = 275$ (at $c_s = 1.5$ mM) and $Z_c = 1100$ (at $c_s = 50$ mM). Corresponding electrostatic free energies per unit area for flat surfaces (g_s) are presented in te ESI.

The SC provides analytical expressions for the interaction between two charged planar surfaces, as well as between two charged spherical particles. Specifically, the PMF (W_{SC}) between two spheres with a common valency, Z_c, and radius, R_c, is given

by:

$$\beta W_{SC}(D) = l_B Z_c^2 \frac{e^{-\kappa D}}{(D+2R_c)(1+\kappa R_c)^2} \quad (16)$$

where l_B is the Bjerrum length, and D (as before) is the surface separation. The corresponding interaction free energy per unit area for planar surfaces, $g_{SC}(D)$, can be written as:

$$\beta g_{SC}(D) = 8 l_B \pi \sigma_s^2 \kappa^{-1} e^{-\kappa D} \quad (17)$$

where σ_s is the surface charge density. The SC force between the particles is naturally obtained from the derivative of W_{SC}, and in the limit of large R_c, the same force is obtained by multiplying g_{SC} with πR_c, in accordance with the DA. Using SC approximations, we can compare the calculated W_{SC} (eq.(16)) with the integrated force, as obtained from g_{SC} (eq.(17)) via the DA (eq. (12)). The former (W_{SC}) are represented by dashed lines in the graphs. The agreement is excellent at high ionic strengths. However, somewhat surprisingly, there is a significant deviation at a salt concentration of 1.5 mM, even though the corresponding Debye screening length (about 78 Å) is almost an order of magnitude smaller than the particle radius. It should be noted that since we are comparing two approximate SC expressions, we cannot conclude that the observed discrepancy is due to the DA being inaccurate. At any rate, the shape of the two SC predictions is very similar, with a difference that in principle could be handled by an adjustment of the particle charge. In other words, the 2-particle SC expression will agree well with that obtained from applying the DA to flat surface predictions, provided that we use a somewhat higher surface charge density in the former case. We have not performed full PB calculations of the PMF between two explicit spheres, as these would be computationally rather demanding. Calculations at flat surfaces or with a single spherical particle, on the other hand, run fast. We will therefore make some further comparisons between SC and full PB with these geometries, in order to scrutinize the observed discrepancies between PB and SC at short separations.

2.2.1 Electrostatic potentials outside an isolated charged particle

Here we will highlight some theoretical predictions for the electrostatic potential, ψ, in the vicinity of an isolated spherical charged particle, of radius $R_c = 600$ Å. Specifically, we shall compare results from calculations using non-linear (PB) and linearized (SC) versions of Poisson-Boltzmann theory. The results are presented in Figure 5. We see that, even with a particle valency of $Z_c = 1000$, there is an excellent agreement between electrostatic profile data from SC and PB calculations. This is despite the fact that $e\beta\psi$ (where e is the elementary charge) exceeds unity close to the surface, i.e. the validity of a linearization is far from obvious. Naturally, for $Z_c = 275$ (our "optimized" value), the agreement is even better.

2.2.2 Electrostatic potentials between charged flat surfaces

Here we will try to provide an explanation to the fact that even though the potential profile outside an isolated particle (or a surface) is accurately reproduced by the linearized PB, the SC approach may still fail to accurately capture the interaction between

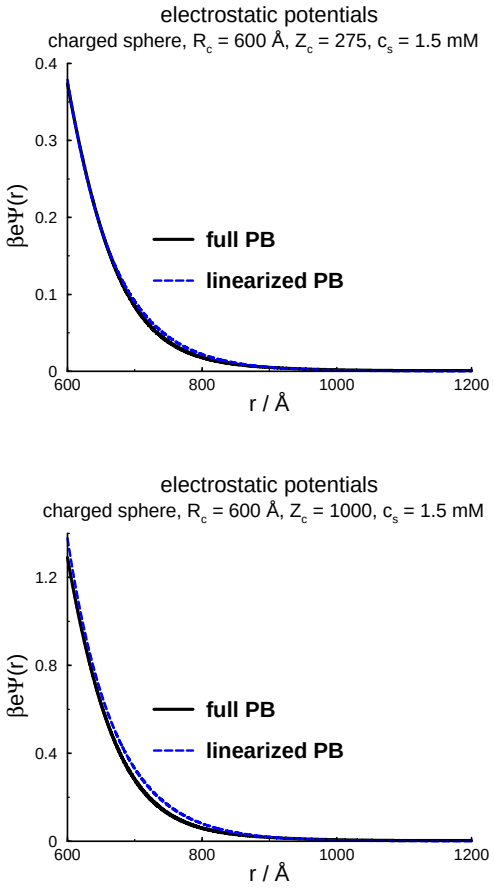

Fig. 5 Comparing theoretical predictions of radially (r) dependent electrostatic potentials outside a spherical particle, of valence Z_c. The salt concentration is $c_s = 1.5$ mM.
(a) $Z_c = 275$ (our "optimized" valency).
(b) $Z_c = 1000$.

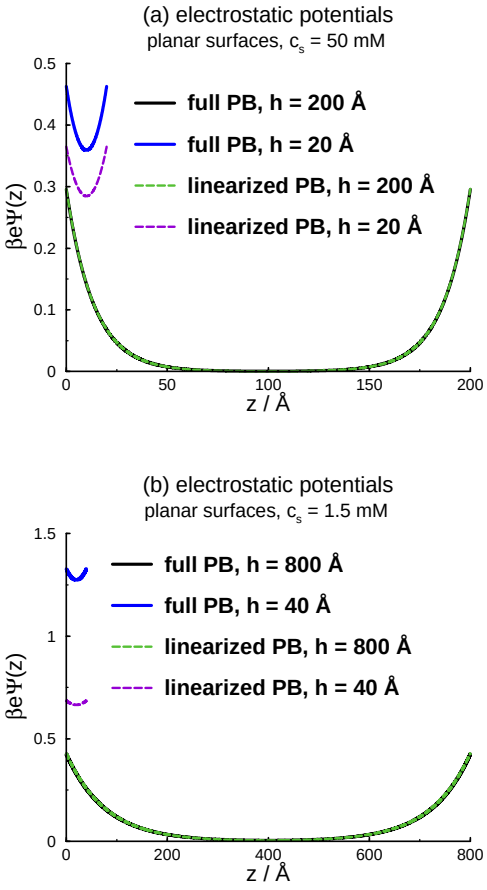

Fig. 6 Comparing theoretical predictions of (z)-dependent electrostatic potentials outside a planar surface (with the z-axis being normal to the surfaces). These comparisons are, for each salt concentration (c_s), performed at a "large" and a "short" separation.
(a) $c_s = 50$ mM. Surface charge density: $\sigma_s = 1100e/(4\pi R_c^2)$, where e is the elementary charge.
(b) $c_s = 1.5$ mM. Surface charge density: $\sigma_s = 275e/(4\pi R_c^2)$.

two such objects. It should be noted that in the latter case, we have used a superposition approximation, adding contributions from two isolated (opposing) surfaces. The results are collected in Figure 6. At both salt concentrations, we find that, in analogy with an isolated charged sphere, the potential profiles from full PB calculations are well captured by an SC model when the surface separation is large. However, as the surfaces are brought close together, the SC becomes highly inaccurate † This is most likely connected to the fact that the inter-surface region becomes almost totally dominated by counterions, which tends to reduce the relevance of the (bulk solution) Debye screening length, κ^{-1}. These effects diminish for small particles, and we have admittedly not made full PB calculations for the interaction between two explicit spherical particles (of radius 600 Å). Such calculations would be computationally demanding (especially in terms of computer memory requirement). Instead, we rely on the validity of the DA approximation, which at least should be very accurate at high salt concentrations.

2.3 Simulations of structure factors

The PMF:s that are established via classical DFT (polymer and PB versions), as outlined above, are imported as tabulated interaction vectors in a canonical Metropolis Monte Carlo code. The simulated particles naturally also have a hard-sphere radius of 600 Å, and the resulting radial distribution functions, $g(r)$, are then Fourier transformed so as to obtain the corresponding "unsmeared" structure factors, $S(q)$, where q is the magnitude of the scattering vector. In order to reduce termination effects, caused by the finite size of our simulation box, we have utilized a standard damping function[53], resulting in:

$$S(q) = 1 + \frac{4\pi N_s R}{8R^3}\int_o^R r^2(g(r)-1)\frac{sin(qr)sin(\frac{\pi r}{R})}{\pi q r^2}dr \qquad (18)$$

where R is half the side length of the cubic simulation box.

The theoretically predicted structure factors can be directly compared with the experimental SAXS data, for particle dispersions without polymer. For a comparison with the SANS data of the particle-polymer mixtures, the calculated structure factors were convoluted with the resolution function, $R(q,Q)$, which accounts for instrument smearing:

$$S_{sm}(q) = \frac{\int S(Q)R(q,Q)dQ}{\int R(q,Q)dQ} \qquad (19)$$

The resolution function is specified in the ESI[12,54].

3 Results and Discussion

3.1 The particle surface charge

Unfortunately, there is no simple and reliable way to experimentally quantify the particle charge, Z_c. We have therefore chosen to use this as a single variable in the model, with a value adjusted

† It is known that the full PB is very accurate under these circumstances (for the given model), i.e. with monovalent salt and low surface charge densities. This has been demonstrated numerous comparisons with corresponding simulation data, where the latter of course are exact, within noise, for the given model.

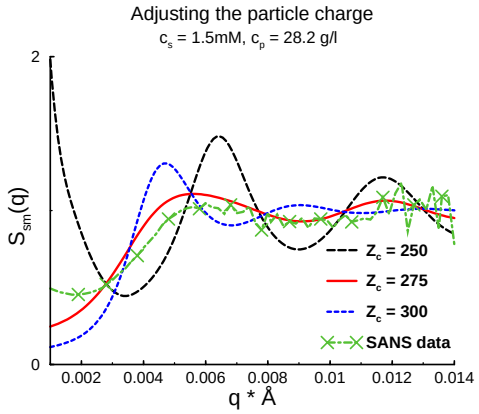

Fig. 7 Comparing experimental data for the structure factor, with c_s =1.5 mM, and c_p =28.2 g/L, with theoretical predictions, for various choices of particle charge, Z_c.

such that gelation is induced at approximately the same polymer concentration as in the corresponding experiments. This value is then kept constant, for all investigated polymer concentrations, at a given value of c_s. For instance, a salt concentration of $c_s = 1.5$ mM, and an overall polymer concentration (c_p) of 28.2 g/L, will bring the system close to the gel point, i.e. the low q regime of $S(q)$ has started to increase rapidly, although not to the point of divergence. In Figure 7, we see that under these conditions $S(q)$ responds rather dramatically to changes of Z_c. Since $S(q)$ modelled with $Z_c = 275$ is closest to the experimental data, we have fixed the particle valency at 1.5 mM salt to 275. In a similar fashion, we have determined $Z_c = 1100$ at 50 mM salt‡. In line with our previous study of MA3 particles under purely repulsive conditions[21], we thus find that the particle charge increases with salt concentration. This is also expected from physical considerations, given that the repulsion between charged groups on the particles will diminish at high levels of salt.

3.2 Structure factors without added polymer

In Figure 8, we compare theoretical predictions and experimental measurements of structure factors, in dispersions containing colloidal particles at various volume fractions, but with no added polymer. In the absence of polymers we can directly compare the model calculations with SAXS data, which display almost no instrumental smearing. The SAXS data agrees quite well with theoretically calculated structure factors, especially for the q-values at which the first structure peak appear. These results contrast with earlier findings for MA3 particles, where an adjustment of the particle charge was required to capture the experimental results[21] at different particle volume fractions (with Z_c varying between 230 and 550). That model was based on a linear PB treatment of electrostatics, and as we have demonstrated above, that leads to a much flatter PMF than predictions from a fully non-linear treatment. Furthermore, a semi-analytical integral equation scheme

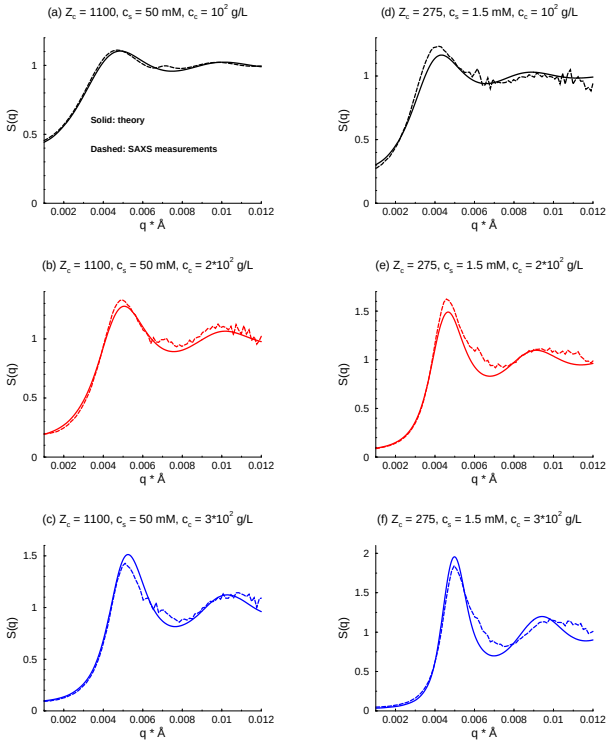

Fig. 8 Structure factors of colloid MA3 in different salt concentrations. Different colors indicate different colloidal particle concentrations c_c. Black: $c_c = 10^2$ g/L ($\phi_c = 0.11$). Red: $c_c = 2 \cdot 10^2$ g/L ($\phi_c = 0.215$). Blue: $c_c = 3 \cdot 10^2$ g/L ($\phi_c = 0.3$). Solid lines represent the theoretical predictions, while dashed lines are SAXS measurements, in a 84/16 H_2O/D_2O solvent mixture.[21]

‡ We estimate that this value also is optimized to within about ±10 %

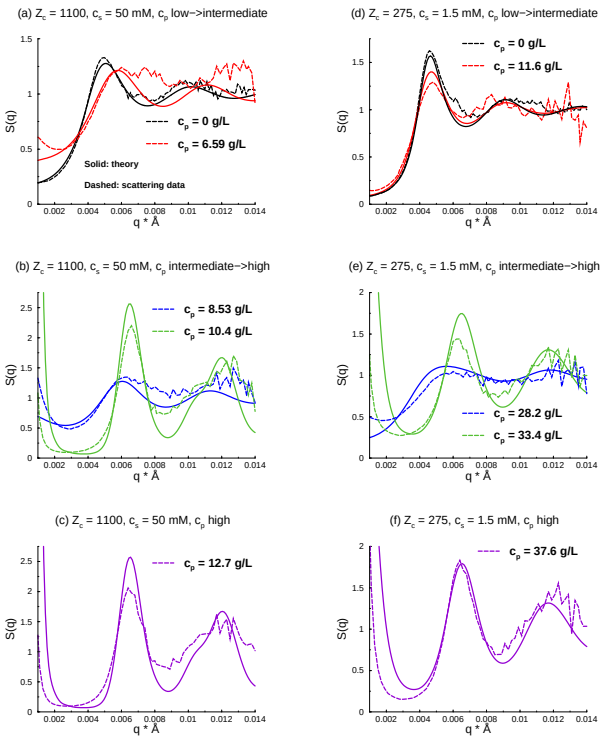

Fig. 9 Theoretical and SANS data for structure factors of colloidal particles MA3, $c_c = 2 \cdot 10^2$ g/L and PEG mixtures. Different colors indicate different polymer concentrations. Solid lines represent the theoretical results, whereas the dashed lines indicate SANS ($c_p > 0$) or SAXS ($c_p = 0$) measurements. Smeared structure factors (S_{sm}) are shown for finite polymer concentrations, since we then compare with SANS data.

was adopted in ref.[21], rather than simulations. It should also be noted that in the absence of attractions, the structure factor becomes less susceptible to (small) changes to the particle charge. It is possible that we would obtain slightly better agreements for these structure factors if we had allowed a varying particle charge, but we have chosen to keep this as a fixed parameter, once it has been optimized with respect to gelation, as described above. Although we cannot fully exclude a volume fraction dependent particle charge, we find that a fixed value gives satisfactory agreement between experimental and theoretical data.

3.3 Structure factors with added polymers

Here we shall test the predictive ability of our theoretical approach, naturally keeping in mind that the particle charge was fitted so as to approximately reproduce the polymer concentrations required to generate gelation. The results in Figure 9 clearly illustrate that the theoretical model reproduces experimental structures for a rather wide range of polymer concentrations. The peaks observed in the regime 0.004 Å$^{-1} < q < 0.007$ Å^{-1} reflect nearest neighbour separations. We note how these peaks move to higher values as polymers are added, indicating how neighbouring particles pack closer together. The peaks not only drift towards higher q values, their amplitudes also varies in a non-monotonic manner. In fact, these peaks almost vanish at intermediate concentrations. This effect is particularly pronounced at low salt concentrations. On the other hand, upon adding large amounts of polymer, the amplitudes of the nearest-neighbour peaks grow quite large. We then also observe a dramatic increase of the structure factor in the low q regime, which signifies a phase transition - in our case gelation. All of these experimentally observed behaviours are semi-quantitatively captured by the theoretical model.

3.4 Radial distribution functions

An obvious advantage with a theoretical model, is that we not only have access to structural information in Fourier space. Radial distribution functions, $g(r)$, are also available. These offer more direct and intuitive structural information. Examples are provided in Figures 10 and 11, at low and high salt, respectively. We see the nearest-neighbour (primary) peak is quite pronounced, even at concentrations significantly below the gelation threshold. At and above this threshold, density peaks of "higher order" (next-nearest neighbour, and so on) develop, and the primary peak becomes extremely strong. These higher-order peaks appear at more well-defined positions when the salt concentration is low, presumably because the electrostatic repulsion favours chain-like structures, rather than random clusters.

3.5 Cluster size distributions

Another way to illustrate the formation of a gel, is to monitor how clusters are formed, and grow as polymers are added.[17] We define a cluster as a collection of particles, where no particle is separated from its nearest neighbour by more than 1250 Å, a distance just beyond the nearest-neighbour peaks in $g(r)$ (see Figures 10 and 11). In Figure 12, we illustrate how the probability $P(k_c)$ for clusters containing k_c colloidal particles, changes as polymers are added to the dispersion. We emphasize that these are only very crude estimates of the true canonically averaged $P(k_c)$, since each cluster distribution is calculated from a single set of coordinates (a simulation snapshot). Nevertheless, while crude, it does serve the purpose of demonstrating that the cluster growth is very dramatic close to the point of gelation, at low as well as at high salt concentrations. Monomers are clearly prevalent at low polymer concentrations, but at and beyond gelation, the average cluster size diverges. This divergence is naturally suppressed in our microscopic system. Specifically, with $N_c = 652$ a cluster can of course at most contain 652 particles. In a macroscopic system, the clusters would essentially grow indefinitely, as expected for a gel.

3.6 Clusters at dilute conditions

We end this work by venturing outside the limits of previously performed experiments, instead providing some as yet untested theoretical predictions. Specifically, we will consider structural effects resulting from a reduction of the particle concentration, in a system with a high polymer concentration. We have simulated a dilute particle system, utilizing the same PMF:s as was established for the previously investigated system with an overall polymer concentration of $c_p = 37.6$ g/l (free volume concentra-

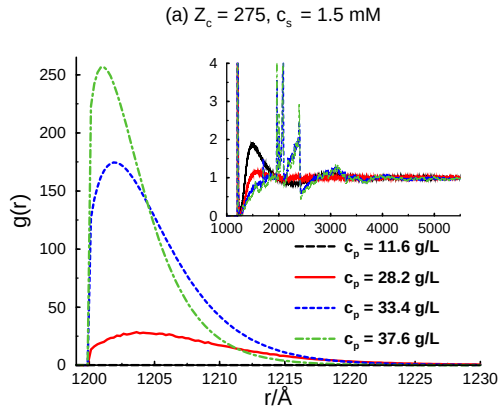

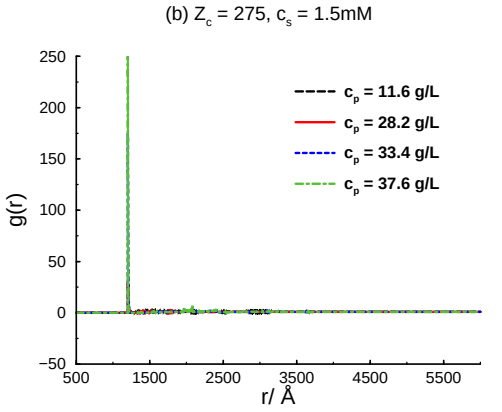

Fig. 10 Radial distribution functions, $g(r)$ between colloidal particles (our model of "MA3"), where r is the distance between particle centres. Results are shown for $c_s = 1.5$mM, at various polymer concentrations, as indicated in the legends.

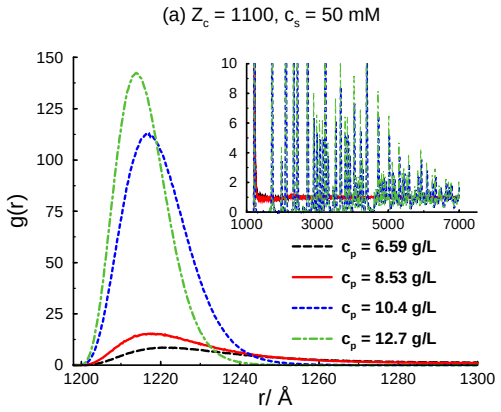

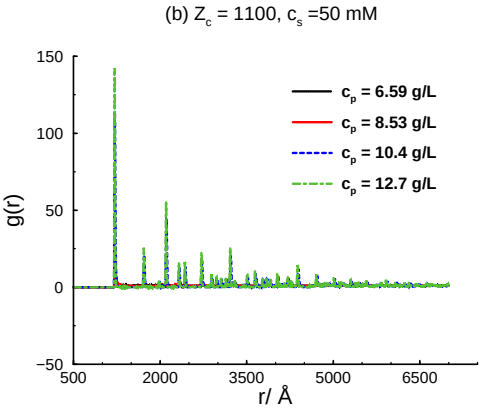

Fig. 11 Radial distribution functions, $g(r)$ between colloidal particles (our model of "MA3"), where r is the distance between particle centres. Results are shown for $c_s = 50$mM, at various polymer concentrations, as indicated in the legends.

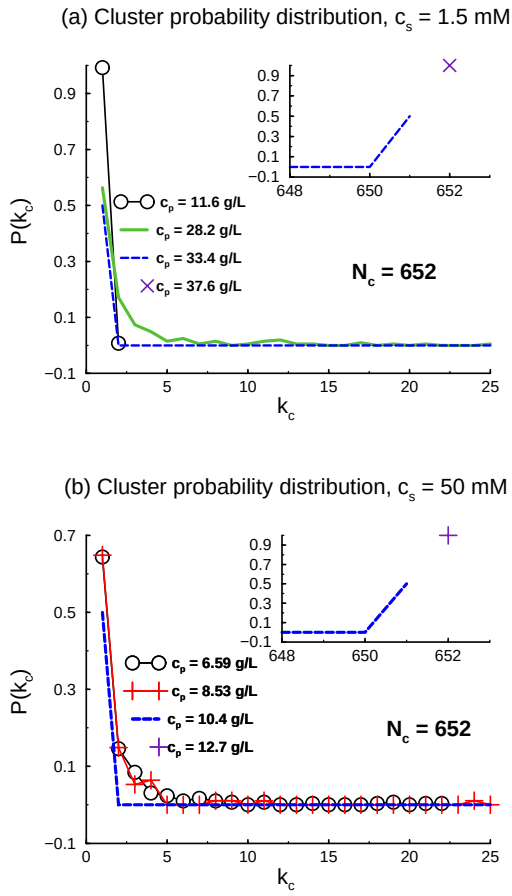

Fig. 12 Crude estimates of cluster size probability distributions, as calculated from single configurations, for various polymer concentrations. The clusters are defined as described in the main text. The simulated number of particles is 652, which sets an (artificial) upper limit for cluster size.
(a) c_s =1.5 mM
(b) c_s =50 mM

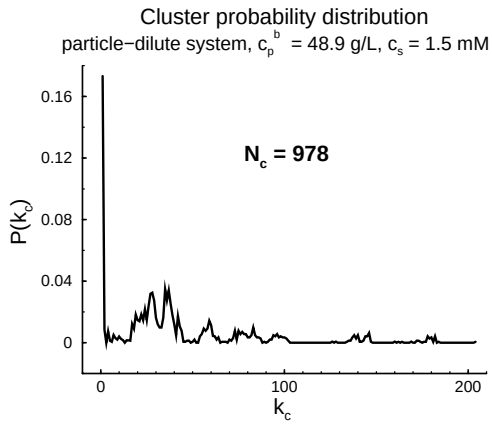

Fig. 13 Cluster size probability distributions, for a system with a low concentration of particles ($\phi_c \approx 0.215/16$), a low concentration of salt ($c_s = 1.5$ mM; Z_c =275), and a high free volume polymer concentration (c_p^b ≈48.9 g/L). The simulated system contained 978 particles, and the threshold cluster radius was set to 1250 (same as in Figure 12).

tion: $c_p^b \approx 48.9$ g/l), and $c_s = 1.5mM$. In our previous simulations, the simulation box contained $N_c = 652$ particles, with a cubic box side length of 14000 Å. Here, we have instead simulated 978 particles, in a box with side length 40383 Å. This corresponds to a 16-fold particle dilution, at a constant salt and bulk polymer concentration.

According to these simulations, a rather interesting phenomenon occurs, in such dilute systems. The system will then not be able to form a space-filling network. Since the interactions are short-ranged compared to the particle size, cluster growth is expected to be an isodesmic process[55] akin to "equilibrium polymerization", although our aggregates are not necessarily linear. In other words, the interaction between two particles is similar to that between a particle and a cluster. At equilibrium, one would then anticipate an exponentially decaying cluster size distribution, $P(k_c)$. [§]. In Figure 13, we have tried to estimate the cluster probability distribution, $P(k_c)$, for this system. In contrast to our previous rather crude description, using a single "snapshot configuration", we have in this case calculated $P(k_c)$ from 70 such snapshots, separated by at least 10 million attempted configurations along the Markov chain. It is nevertheless somewhat noisy. However, the main conclusion is clear, namely that in this system we end up with a range of finite-sized clusters, which, at least in the absence of gravitational effects, will resist complete phase separation into separate dilute and concentrated phases. Unfortunately, we have not been able to simulate long enough, and with a sufficiently large system size, to verify the expected exponential decay of $P(k_c)$.

In Figure 14 we display a configuration snapshot, illustrating how a range of isolated clusters, of various sizes typically exist.

§ This is in contrast to the scenario in systems with long-ranged interactions (compared to the particle size), in which case a liquid-gas equilibrium will be established.

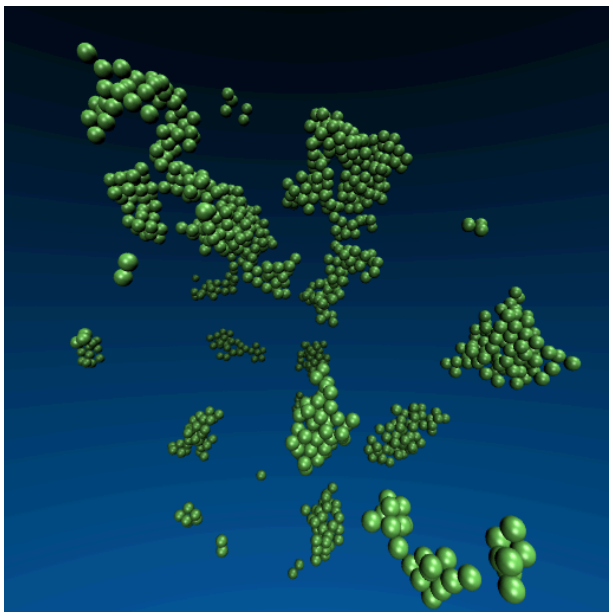

Fig. 14 A snapshot of our simulated dilute system (see text, and captions to Figure 13).

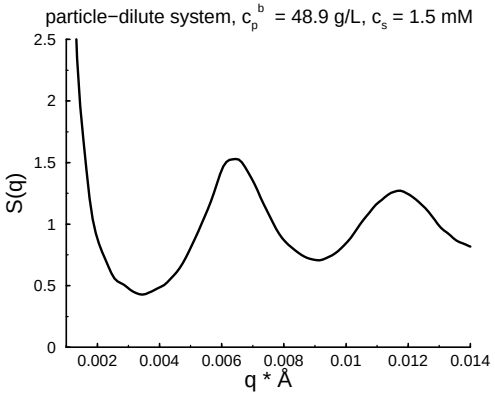

Fig. 15 Predicted structure factor, for our simulated dilute system (see text, and captions to Figure 13).

Interestingly, the structure factor itself seems unable to distinguish between these structures, and the ones obtained for a space-spanning gel network, at higher particle volume fractions. This is highlighted in Figure 15.

4 Conclusions

In this work, we have attempted to quantify the interactions that govern the structural behaviour of a particle/polymer mixture. The specific system, containing charged polystyrene particles, and added PEG polymers, has been investigated experimentally, via scattering analyses, in an earlier study [27]. We have made efforts to construct a model that contains the relevant physics, yet is coarse-grained enough to be rather easily evaluated using simple theoretical methods. Specifically, we have used classical polymer density functional theory (DFT) to calculate the depletion interactions that the non-adsorbing PEG molecules mediate. This approach has the advantage that all configurations are accounted for, subject to a mean-field Boltzmann weight. We have implemented ways to correct for inaccuracies resulting from the mean-field assumption, and utilize a PEG model that has been shown to accurately reproduce bulk osmotic pressures as well as the isolated chain radius of gyration. We have demonstrated that the DFT is able to accurately capture the drop in correlation length that results from an increase of the polymer concentration. Importantly, the reduced correlation length also results in a decreased range of the depletion interaction. Furthermore, the electrostatic interactions are calculated at the fully non-linear Poisson-Boltzmann level, rather than its commonly used linearized version. We have shown that the latter approach results in a significant loss of accuracy, especially for close particle-particle encounters, which is a regime that is crucial to the development of a gel. The theoretical particle charges are adjusted such that gelation in the model occurs for similar polymer concentrations as is found experimentally. Our theoretical predictions for the structure factors agree with corresponding experimental data, for a range of polymer concentrations, and at low as well as high salt levels. We furthermore explore other structural aspects of the gelation process, such as radial distribution functions, and cluster size distributions.

Finally, we use our model to make predictions for the behaviour of similar dispersions, but at much lower particle concentrations. We find that gelation then is suppressed (at least in absence of gravitational effects), and that a polydisperse distribution of equilibrium clusters are formed. Interestingly, the structure factor of such a dispersion is very similar to that found in a gel system, at much higher particle concentrations, but at low salt. It would be interesting to test these predictions experimentally, with the caveat that such highly polydisperse equilibrium clusters may be difficult to verify and analyze. [19]

5 Acknowledgment

J. F. acknowledges financial support by the Swedish Research Council. K.v.G. and A.S. gratefully acknowledge beam time for the SANS and SAXS experiments performed on the SANS-I instrument at the Swiss spallation neutron source SINQ and the cSAXS beamline at the Swiss Light Source SLS, Paul Scherrer Institut,

Villigen, Switzerland.

References

1 A. Donald, *Nature Materials*, 2004, **3**, 579–581.
2 N. A. Verhaegh, D. Asnaghi, H. N. Lekkerkerker, M. Giglio and L. Cipelletti, *Physica A: Statistical Mechanics and its Applications*, 1997, **242**, 104 – 118.
3 W. C. K. Poon, *J. Phys.: Cond. Mat.*, 2002, **14**, R859.
4 R. Mezzenga, P. Schurtenberger, A. Burbidge and M. Michel, *Nature Materials*, 2005, **4**, 729–740.
5 L. Belloni, *J. Phys.: Cond. Mat.*, 2000, **12**, R549.
6 P. N. Segrè, V. Prasad, A. B. Schofield and D. A. Weitz, *Phys. Rev. Lett.*, 2001, **86**, 6042–6045.
7 M. Quesada-Perez, J. Callejas-Fernandez and R. Hidalgo-Alvarez, *Adv. Coll. Int. Sci.*, 2002, **95**, 295 – 315.
8 P. Lu, E. Zaccarelli, F. Ciulla, A. B. Schofield, F. Scortino and D. A. Weitz, *Nature*, 2008, **453**, 499–503.
9 W. K. Lim and A. R. Denton, *J. Chem. Phys.*, 2014, **141**, 114909.
10 W. K. Lim and A. R. Denton, *J. Chem. Phys.*, 2016, **144**, 024904,.
11 W. K. Lim and A. R. Denton, *Soft Matter*, 2016, **12**, 2247–2252.
12 J. S. Pedersen, *J. Phys. IV*, 1993, **3**, 491–498.
13 R. Hidalgo-Alvarez, A. Martin, A. Fernandez, D. Bastos, F. Martinez and F. de las Nieves, *Adv. in Coll. and Int. Sci.*, 1996, **67**, 1 – 118.
14 G. Nägele, *Physics Reports*, 1996, **272**, 215 – 372.
15 C. Beck, W. Härtl and R. Hempelmann, *J. Chem. Phys.*, 1999, **111**, 8209–8213.
16 S. H. Behrens, D. I. Christl, R. Emmerzael, P. Schurtenberger and M. Borkovec, *Langmuir*, 2000, **16**, 2566–2575.
17 A. Stradner, H. Sedgwick, F. Cardinaux, W. C. K. Poon, S. U. Egelhaaf and P. Schurtenberger, *Nature*, 2004, **432**, 492–495.
18 S. A. Shah, S. Ramakrishnan, Y. L. Chen, K. S. Schweizer and C. F. Zukoski, *Langmuir*, 2003, **19**, 5128–5136.
19 C. P. Royall, D. G. A. L. Aarts and H. Tanaka, *J. Phys.: Cond. Mat.*, 2005, **17**, S3401.
20 H. Sedgwick, J. E. Cameron, W. C. K. Poon and S. U. Egelhaaf, *J. Chem. Phys.*, 2007, **127**, 125102.
21 K. van Gruijthuijsen, M. Obiols-Rabasa, M. Heinen, G. Nägele and A. Stradner, *Langmuir*, 2013, **29**, 11199–11207.
22 P. N. Pusey and W. van Megen, *Nature*, 1986, **320**, 340 – 342.
23 C. P. Royall, W. C. K. Poon and E. R. Weeks, *Soft Matter*, 2013, **9**, 17–27.
24 B. V. Derjaguin, *Kolloid Zeits.*, 1934, **69**, 155.
25 K. van Gruijthuijsen, R. Tuinier, J. M. Brader and A. Stradner, *Soft Matter*, 2013, **9**, 9977–9982.
26 K. van Gruijthuijsen, W. G. Bouwman, P. Schurtenberger and A. Stradner, *EPL*, 2014, **106**, 28002.
27 F. Xie, M. Turesson, M. Jansson, M. Skepö and J. Forsman, *Polymer*, 2016, **84**, 132 – 137.
28 S. Asakura and F. Oosawa, *J. Chem. Phys.*, 1954, **22**, 1255–1256.
29 W. B. Russel, D. A. Saville and W. R. Schowalter, *Colloidal Dispersions*, Cambridge University Press, 1989.
30 H. N. W. Lekkerkerker and R. Tuinier, *Colloids and the Depletion Interaction (Lecture Notes in Physics)*, Springer, 2011.
31 C. E. Woodward, *J. Chem. Phys.*, 1991, **94**, 3183.
32 C. E. Woodward and A. Yethiraj, *J. Chem. Phys.*, 1994, **100**, 3181.
33 J. Forsman and C. E. Woodward, *Macromol*, 2007, **40**, 8396.
34 K. G. Honnell and C. K. Hall, *J. Chem. Phys.*, 1991, **95**, 4481.
35 S. Nordholm, M. Johnson and B. C. Freasier, *Aust. J. Chem.*, 1980, **33**, 2139.
36 M. Turesson, J. Forsman and T. Åkesson, *Phys. Rev. E*, 2007, **76**, 021801.
37 P. J.A.Cohen, R.Podgornik and V.A.Parsegian, *J.Phys Chem*, 2009, **113**, 3709–3714.
38 K. G. Honnell and C. K. Hall, *J. Chem. Phys.*, 1989, **90**, 1841.
39 Q. Ying and B. Chu, *Macromol.*, 1987, **20**, 362–366.
40 J. Forsman, *J. Phys. Chem. B*, 2004, **108**, 9236.
41 S. Asakura and F. Oosawa, *J. Polym. Sci.*, 1958, **33**, 183.
42 A. Vrij, *Pure Appl. Chem.*, 1976, **48**, 471.
43 H. N. W. Lekkerkerker, W. C. K. Poon, P. N. Pusey, A. Stroobants and P. B. Warren, *Europhys. Lett.*, 1992, **20**, 559.
44 H. N. W. Lekkerkerker and A. Stroobants, *Physica A*, 1993, **195**, 387.
45 M. Dijkstra, R. van Roij and R. Evans, *Phys. Rev. E*, 1999, **59**, 5744.
46 R. P. Sear, *Phys. Rev. Lett.*, 2001, **86**, 4696.
47 R. Tuinier, J. Rieger and C. G. de Kruif, *Adv. Coll. Int. Sci.*, 2003, **103**, 1.
48 M. Dijkstra, R. van Roij, R. Roth and A. Fortini, *Phys. Rev. E*, 2006, **73**, 041404.
49 B. Widom and J. S. Rowlinson, *J. Chem. Phys.*, 1970, **52**, 1670–1684.
50 H. N. W. Lekkerkerker, *Colloid Surf.*, 1990, **51**, 419.
51 J. Forsman and C. E. Woodward, *J. Chem. Phys.*, 2009, **131**, 044903.
52 F. Xie, M. Turesson, M. Jansson, M. Skepö and J. Forsman, *Polymer*, 2016, **84**, 132 – 137.
53 E. Lorch, *Journal of Physics C: Solid State Physics*, 1969, **2**, 229.
54 B. Hammouda and D. F. R. Mildner, *J. Appl. Cryst.*, 2007, **40**, 250–259.
55 T. F. A. de Greef and E. W. Meijer, *Nature*, 2008, **453**, 171–173.